

# Estimating Net Ecosystem Exchange of Carbon Using the Normalized Difference Vegetation Index and an Ecosystem Model

F. Veroustraete,<sup>\*</sup> J. Patyn,<sup>\*</sup> and R. B. Myneni<sup>†</sup>

*The evaluation and prediction of changes in carbon dynamics at the ecosystem level is a key issue in studies of global change. An operational concept for the determination of carbon fluxes for the Belgian territory is the goal of the presented study. The approach is based on the integration of remotely sensed data into ecosystem models in order to evaluate photosynthetic assimilation and net ecosystem exchange (NEE). Remote sensing can be developed as an operational tool to determine the fraction of absorbed photosynthetically active radiation (fPAR). A review of the methodological approach of mapping fPAR dynamics at the regional scale by means of NOAA11-AVHRR/2 data for the year 1990 is given. The processing sequence from raw radiance values to fPAR is presented. An interesting aspect of incorporating remote sensing derived fPAR in ecosystem models is the potential for modeling actual as opposed to potential vegetation. Further work should prove whether the concepts presented and the assumptions made in this study are valid.*

(NEE). Complex ecosystem models with a highly predictive value for a specific ecosystem are generally not suitable for global or regional applications, since they require a substantial set of ancillary data becoming increasingly larger with increasing complexity of the model. The ideal model for our purpose is one that is simple enough to be used in global scale modeling, and which can be adapted for different ecosystems or vegetation types. The fraction of absorbed photosynthetically active radiation (fPAR) during the growing season determines in part net photosynthesis and phytomass production (Ruimy, 1995). Remotely measured red and near-infrared spectral reflectances can be used to estimate fPAR. Therefore, a possible approach is to estimate net photosynthesis, phytomass, and NEE from a combination of satellite data and an ecosystem model that includes carbon dynamics. It has to be stated that some parts of the work presented in this publication are a description of concepts. Other parts are descriptions of methodology and case studies of the concepts developed.

## INTRODUCTION

The importance of vegetation in global carbon cycling is well recognized. The determination of whether vegetation is a net source or sink of carbon is the objective of this study. Our approach is to incorporate remote sensing data into ecosystem models to evaluate photosynthetic assimilation and net ecosystem exchange

## THE BELFIX PROCEDURE

Figure 1 gives an overview of the Belfix (Belgian carbon fixation) procedure and its segments. Raw digital counts from NOAA11-AVHRR/2 are geometrically rectified, radiometrically calibrated, and atmospherically corrected. Top-of-the-canopy normalized difference vegetation index (TOC NDVI) is thus calculated on a yearly basis. This index is converted to fPAR on a pixel per pixel basis. A Fourier series model is fitted through a yearly series of fPAR to force the ecosystem model and also to derive a set of discriminant parameters (based on the differences in temporal dynamics of fPAR) to be used in a cluster analysis to classify vegetation using a geographical information system. The vegetation clusters correspond with a functional type (FT). The similar-

<sup>\*</sup>Centre for Teledetection, Energy Department, Flemish Institute for Technological Research (VITO), Boeretang, Belgium

<sup>†</sup>Biospheric Sciences Branch, Goddard Space Flight Center, Greenbelt, USA

Address correspondence to F. Veroustraete, Energy Dept., Flemish Inst. for Technological Research, Boeretang 200, B-2400, Mol, Belgium.

Received 15 April 1994; revised 4 December 1995.

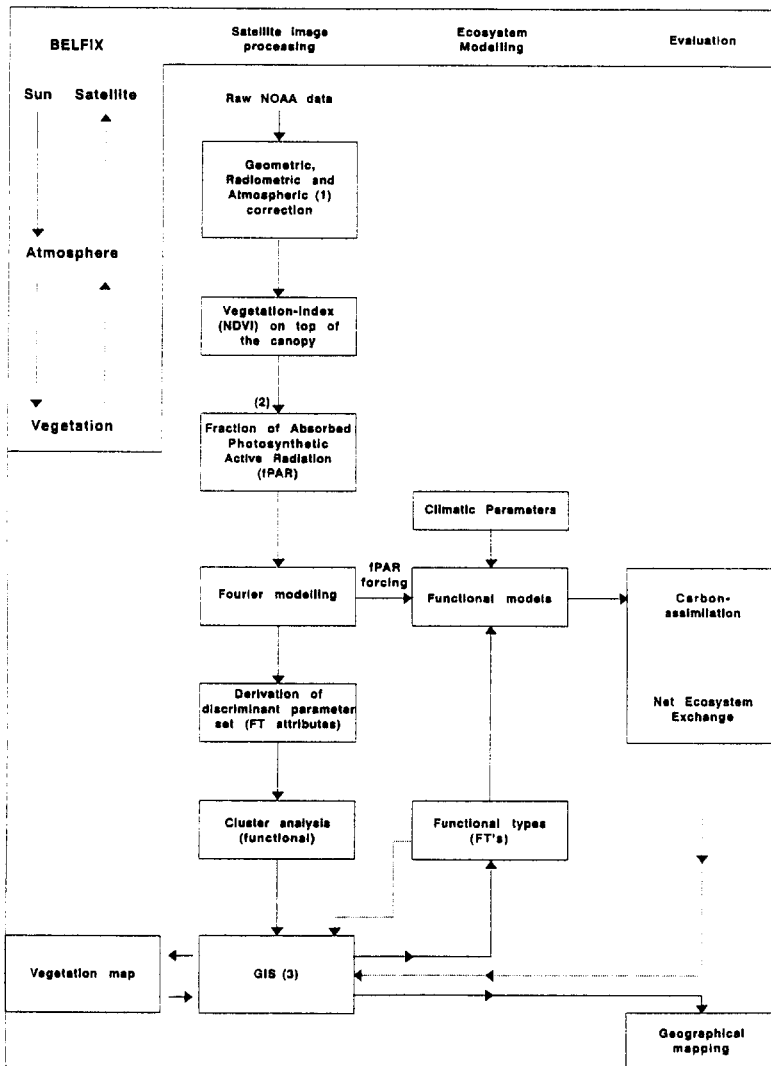


**Figure 1.** Summary of the BELFIX procedure. The procedure is divided in three subsections: satellite image processing, ecosystem modelling, and evaluation. The satellite image processing section starts with raw NOAA data which subsequently are processed to obtain fPAR. Geometric rectification of images, radiometric and atmospheric corrections are performed. Subsequently the NDVI on top of the canopy is converted into fPAR. The models used are indicated in the legend. Yearly fPAR profiles are subsequently fitted with a Fourier series model. In a first branch, Fourier model results are used to derive a set of discriminant parameters (FT attributes), which, on a pixel per pixel basis, are used in cluster analysis to map functional types for Belgium. In GIS cluster maps of FTs are compared with a digital vegetation map (results of this branch of the procedure are not described in this publication). Finally in a second branch, functional ecosystem models, representative for a certain functional type (in this publication, temperate zone deciduous forest), are forced with daily fPAR values and hourly climatological parameters to evaluate carbon assimilation and net ecosystem exchange of carbon, which can then be mapped in GIS. Legend: 1) atmospheric correction: dark pixel subtraction; 2) radiation transfer model at vegetation level (3D model from Myneni); 3) geographical Information System (Arc / Info).

ity of a functional type with a structural vegetation type is investigated with a digital land use map derived from ground observations.

It will not be feasible to develop models for every ecosystem, globally or even regionally. Thus, the concept that the complexity of nature can be reduced in models by treating a smaller number of FTs is an essential step. A functionally oriented (as opposed to a phenetic or phylogenetic) classification is an effective way of reducing the complexity of ecosystem process modelling. It has often been argued that the essential dynamics of ecosystems can be captured by grouping species into a restricted number of FTs (Grime, 1979; Noble and Slatyer, 1980; Woodward, 1987). Classically the FT approach is based on a minimum set of functional attributes that are considered to be most critical in reliably predicting the distribution of plants from climatic input variables. This set of attributes (e.g., frost resistance, phenology, longevity, etc.) defines an FT. The entities (e.g., species) that possess the same set of attributes are all classified in the same FT. The emphasis on a mini-

mum set of functional attributes allows the global scope of the approach, with a strong avoidance of nonessential attributes that are of secondary or lower importance. Simple rules therefore are essential to recognize FTs. It will be the subject of another publication to elaborate further on the derivation of the discriminant attributes derived from yearly fPAR dynamical differences in order to define FTs.

Only those functional types exhibiting geographical correspondence with structurally identified vegetation types will be used for ecosystem modeling purposes. This process is repeated until optimal coverage for Belgium is obtained, that is, maximal geographical correspondence between vegetation and functional type maps. Ecosystem models will be developed for each of the functional types to be able to model carbon exchange for the Belgian territory. One such model, for deciduous forests, has been developed as a test case for fPAR forcing (Veroustraete, 1994a,b). Carbon assimilation, mapping of photosynthetic assimilation and NEE will be performed with the ecosystem model on a pixel per

Table 1. NOAA11-AVHRR / 2 Scenes for 1990 Used in This Study<sup>a</sup>

Scene	Date	Day	Overh Time GMT	Col. Pos	Col. No.	Eqx. East	Eqx Time GMT	Orbit No.	Orbit Direction	Remarks
856-04A	18.01.1990	18	12:57	801	451	18.70	12:41:58	6785	Asc.	Cloudless
859-09B	05.01.1990	36	13:06	996	450	16.01	12:50:42	7039	Asc.	Cloudless
859-12A	06.02.1990	37	12:55	733	450	19.48	12:39:47	7052	Asc.	Clouds Westhoek, coast, North Sea
862-13A	22.02.1990	53	13:25	1313	390	12.19	13:09:49	7279	Asc.	Cloudless
863-01B	23.02.1990	54	13:14	1131	450	14.93	12:58:55	7293	Asc.	Cloudless
866-05A	12.03.1990	71	13:33	1453	450	10.48	13:17:36	7533	Asc.	Clouds NE Limburg, Herve
866-12B	15.03.1990	74	13:00	821	450	18.72	12:44:50	7575	Asc.	Cloudless
867-01A	16.03.1990	75	12:50	621	450	21.46	12:33:53	7589	Asc.	Cloudless
867-03B	17.03.1990	76	12:39	431	450	24.21	12:22:59	7603	Asc.	Cloudless
867-06B	18.03.1990	77	12:29	313	450	26.96	12:12:03	7617	Asc.	Cloudless
869-10B	30.03.1990	89	13:40	1491	450	8.90	13:24:56	7787	Asc.	Cloud veil coastal area
869-13A	31.03.1990	90	13:29	1401	450	11.65	13:13:59	7801	Asc.	Cloudless
870-01B	01.04.1990	91	13:19	1173	450	14.40	13:03:01	7815	Asc.	Cloudless
871-08B	09.04.1990	99	13:33	1413	450	10.96	13:17:24	7928	Asc.	Clouds SE-Ardenne
875-03A	29.04.1990	119	13:17	1111	450	15.15	13:01:44	8210	Asc.	Cloudless
875-05B	30.04.1990	120	13:06	881	450	17.92	12:50:43	8224	Asc.	Cloudless
875-13A	03.05.1990	123	12:34	321	450	26.23	12:17:41	8266	Asc.	Cloudless
878-10B	18.05.1990	138	13:12	971	450	16.81	12:56:24	8478	Asc.	Cloud veils N-Belgium, Antwerp, Gent, coast, Southern Ardenne
880-11A	29.05.1990	149	12:53	591	450	21.80	12:36:58	8633	Asc.	Clouds coastal area
889-01B	13.07.1990	194	13:05	751	450	19.45	12:49:11	9268	Asc.	Cloudless
890-03A	19.07.1990	200	13:40	1451	450	10.69	13:24:40	9353	Asc.	Cloudless
809-08A	21.07.1990	202	13:18	1026	450	16.27	13:02:31	9381	Asc.	Cloudless
891-14B	29.07.1990	210	13:31	1271	450	13.03	13:15:51	9494	Asc.	Partial cloud formations, N- and E-Belgium and Lotharingen
892-10B	02.08.1990	214	12:48	453	450	24.21	12:31:28	9550	Asc.	Cloudless
896-14A	24.08.1990	236	13:49	1566	450	9.21	13:33:15	9861	Asc.	Cloudless
906-01B	12.10.1990	285	13:12	801	450	19.05	12:56:46	10552	Asc.	Cloudless

<sup>a</sup> Legend: Asc = ascending node satellite orbit (from south to north). Overhead times are indicative for DUNDEE (UK) with an accuracy of ± 1 min GMT (P. Baylis, Dundee satellite station, personal communication). Column position gives the pixel column from east to west for the starting point of cutouts for Belgium. Col. No. gives the number of columns for a total scene of Belgium. The terminology cloudless must be interpreted as "No clouds present in the region of interest for this study, based on visual inspection."

pixel basis, with yearly temporal fPAR profiles obtained from Fourier modeling.

The presented scheme is partially operational. The satellite image processing sequence is operational to the level of Fourier modeling and the conversion of TOC NDVI to fPAR has been established, using a 3D radiation transfer model. In this article, the processing of remote sensing data, the relationship between TOC NDVI and fPAR, regional fPAR mapping, and forcing of an ecosystem model for deciduous forest with remote sensing derived fPAR will be presented.

**CORRECTION OF NOAA11-AVHRR / 2 DATA**

**Geometric Rectification**

From a total of 85 NOAA11-AVHRR / 2 images in 1990, 26 cloudless scenes were selected. For a definition of the term cloudless, see the legend of Table 1. The accuracy of image rectification was based on the 26

selected images. Table 1 summarizes the acquisition dates and orbital characteristics of the scenes.

Nonparametric approaches of image rectification with interpolation methods are independent of the choice and location of ground control points (GCPs). The goal of image rectification is to match the nonrectified image (NRI) with a rectified image (RI). The matching is done by mathematical transformation of the abscissa of selected GCPs. Consequently, the pixels of the NRI are geometrically transformed to the RI pixel format. The final step is resampling, where the new radiance or digital reflectance values are reallocated in the RI on the basis of the transformed NRI. The use of polynomials in image rectification assumes that maps are available for the region of interest. Two Cartesian coordinate systems are defined. One describes the location of the GCP coordinates on the RI (x, y), and the other coordinate system defines the location of the pixels in the original image (u, v), the NRI. One starts from

the assumption that the two coordinate systems can be related by means of mapping functions  $f$  and  $g$ :

$$u = f(x, y) + r_u, \quad (1)$$

$$v = g(x, y) + r_v, \quad (2)$$

where  $r_u$  and  $r_v$  are the residuals of  $n$  GCPs. The application of a minimization procedure on the root mean square errors of the X and Y pixels allows for the calculation of mapping functions with minimal residuals. In general, more GCPs are chosen than strictly necessary to increase the accuracy of rectification.

With the aforementioned functions, the pixels can be localized by means of their position on the map. Polynomials of first, second, and third order are generally chosen as mapping functions:

$$u = a_0 + a_1x + a_2y + (a_3xy + a_4x^2 + a_5y^2) + r_u, \quad (3)$$

$$v = b_0 + b_1x + b_2y + (b_3xy + b_4x^2 + b_5y^2) + r_v. \quad (4)$$

The mapping functions ( $u$  and  $v$ ) can be applied to relate each pixel from the NRI with the RI coordinates after the coefficients  $a_i$  and  $b_i$  are evaluated. The values of the coefficients are determined by the location of the GCPs. These are spatially well-recognizable points, like coastlines, rivers, lakes, etc. The minimal number of GCPs for a first-order polynomial is three, and six for a second-order polynomial. In practice, however, more GCPs are chosen to allow for residual minimization. When the residuals have a magnitude of approximately one pixel, the transformed image is assumed accurately rectified. This approach was implemented for the 26 NOAA11 scenes of the Belgian territory.

#### Selection of the Ground Control Points

Well-defined GCPs were selected for accurate image rectification and to generate polynomial coefficients such that the rectified image corresponds to cartographic reality. A general rule is to select GCPs at the edges of a well-defined region. In addition, GCPs must be homogeneously distributed over the territory. The order of polynomials must be carefully chosen. As a rule polynomials of higher order are more precise in the neighborhood of the GCPs but not necessarily in areas between the GCPs. When for example due to partial cloud cover, GCPs cannot be identified in the NRI, higher-order polynomials will result in less precise image rectification. The coordinate system chosen for the rectified image is the Belgian Lambert network (Prils, 1989). This enables comparisons and correlation studies with vegetation or topographical maps. The coordinates of the GCPs, located with an accuracy of 100 meters, were determined by means of topographical maps prepared by the Belgian National Geographical Institute (NGI) at a scale of 1 / 10,000.

#### Accuracy of the Image Rectification

Table 2 summarizes root mean square error (RMSE) values of the residuals after geometrical rectification for

Table 2. Summary of RMSE Values<sup>a</sup>

Scene	RMSE <sub>x</sub>	RMSE <sub>y</sub>	RMSE <sub>Tot</sub>
856-04A	1.0	1.2	1.6
859-09B	2.2	2.6	3.4
859-12A	3.9	1.0	4.0
862-13A	1.6	0.6	1.7
863-01B	1.2	2.0	2.4
866-05A	1.1	1.3	1.7
866-12B	1.5	1.2	1.9
867-01A	3.1	0.9	3.2
867-03B	1.8	1.2	2.2
867-06B	3.0	1.1	3.2
869-10B	1.7	2.1	2.7
869-13A	2.7	1.2	3.0
870-01B	2.3	1.9	3.0
871-08B	1.9	2.3	3.0
875-03A	1.9	1.6	2.5
875-05B	3.1	1.6	3.5
875-13A	1.9	1.3	2.3
878-10B	1.0	1.0	1.4
880-11A	3.4	1.1	3.5
889-01B	1.4	1.6	2.1
890-03A	2.3	2.4	3.3
890-08A	2.9	1.5	3.2
891-14B	0.7	0.9	1.1
892-10B	2.4	1.2	2.7
896-14A	2.0	1.3	2.4
906-01B	2.9	0.9	3.1
Mean RMSE	2.1	1.4	2.6

<sup>a</sup> Legend: Xpix: GCP pixel position in X direction (from east to west). Ypix: GCP pixel position in Y direction (from south to north). Th: theoretical coordinate of GCP obtained with the polynomial model. n: number of GCPs used in the rectification (variable according to cloudiness, with a maximum of 11). p: number of coefficients of the polynomial used (e.g., 3).

$$RMS_x = \sqrt{\frac{\sum(Xpix - Xpix_{Th})^2}{n - p}}, \quad RMS_y = \sqrt{\frac{\sum(Ypix - Ypix_{Th})^2}{n - p}},$$

$$RMS_{Tot} = \sqrt{\frac{\sum((Xpix - Xpix_{Th})^2 + (Ypix - Ypix_{Th})^2)}{n - p}}.$$

the 26 images in 1990 for Belgium. The results indicate that the residuals are larger in the X coordinate than the Y coordinate. The RMSEs of the absolute values of X and Y residuals are 1.73 and 1.09 pixels, respectively. Cracknell and Paithoonwattanakij (1989) obtained standard deviations on the X- and Y-coordinates of 0.974 km and 0.704 km, respectively, and mean deviations of the absolute values on the X- and Y-residuals of 0.82 and 0.60 pixels, after application of an orbital model and subsequent rectification with GCPs. Their results also, show a larger deviation in the X as opposed to the Y coordinate. One of the reasons for higher residual values in our case is the manual location of the GCPs in the NRIs. Navigational information was not used in this study, since the region of interest (Belgium) is only a small subset of a NOAA scene, only GCPs were used to rectify the imagery.

#### Resampling

Even after rectification, a pixel in an RI does not necessarily coincide with its location in the reference (topo-

Table 3. Chi-Square Test for a Fit of an Exponential Function through the Histograms of the Residuals in the X Direction (a) and Y Direction (b)<sup>a</sup>

Residual Intervals in Pixels	Observed Frequency	Expected Frequency	Chi-Square
(a)			
< 0.4	49	56.8	1.0774
0.4–0.8	37	45.1	1.463
0.8–1.2	35	35.8	0.019
1.2–1.6	48	28.5	13.422
1.6–2.0	28	22.6	1.291
2.0–2.4	12	17.9	1.970
2.4–2.8	15	14.3	0.039
2.8–3.2	20	11.3	6.663
3.2–3.6	7	9.0	0.439
3.6–4.0	6	7.1	0.181
4.0–4.4	3	5.7	1.255
4.4–5.2	5	8.1	1.170
5.2–6.0	4	5.1	0.234
> 6.0	7	8.7	0.330
(b)			
< 0.24	52	54.4	0.105
0.24–0.56	48	56.2	1.203
0.56–0.88	44	42.0	0.099
0.88–1.20	39	31.3	1.886
1.20–1.52	25	23.4	0.114
1.52–1.84	19	17.4	0.139
1.84–2.16	15	13.0	0.303
2.16–2.48	14	9.7	1.892
2.48–2.80	6	7.2	0.215
2.80–3.12	6	5.4	0.064
3.12–3.76	1	7.1	5.192
> 3.76	7	8.9	0.391

<sup>a</sup> Legend: Fitted functions:  $Y = e^{-\beta_x X}$  (a),  $Y = e^{-\beta_y Y}$  (b), where  $Y$  is the frequency and  $X$  the number of pixels.  $\beta_x = 1.73$ , chi-square = 29.5 with 12 degrees of freedom, significance level = 0.00326.  $\beta_y = 1.09$ , chi-square = 11.6 with 10 degrees of freedom, significance level = 0.312.

graphical) map due to transformation errors. Therefore, a decision has to be made concerning pixel NDVI value in the RI. The original pixel NDVI values were resampled by taking into account the frequency distributions of the X- and Y-pixel residuals. An exponential model fits the frequency distributions accurately (Table 3). In the resampling procedure, a weight is assigned to the neighboring pixels as determined by the biexponential density function  $b(x, y)$ . This function is described according to

$$NDVI_n = \sum_x \sum_y \omega_i \cdot NDVI_i \quad \text{with} \quad \sum_x \sum_y \omega_i = 1, \quad (5)$$

where  $\omega_i$  is the weighting factor according to the biexponential function  $b(x, y)$ :

$$b(x, y) = e^{-x/\beta_x - y/\beta_y} \quad (6)$$

$\beta_x$  and  $\beta_y$  equal the RMSEs of the absolute values of X and Y residuals, respectively. This method ensures maximal conservation of the original pixel NDVI value, by taking into account the actual accuracy of image rectification.

### Radiometric Calibration

The AVHRR sensors of the NOAA series of satellites do not dispose of on-board calibration facilities for Channels 1 and 2 (Channel 1, VIS and 2, NIR). One therefore has to rely on either prelaunch calibration coefficients (gain and offset), or ground-based absolute calibration coefficients. Raw satellite data were converted into spectral radiance values by means of prelaunch calibration factors, equivalent band widths, and integrated solar spectral irradiance weighted by the relative spectral response function of the sensor wavelength band for the red and near-infrared channels.

The following relationship was applied to obtained spectral radiance values for the VIS and NIR bands on top of the atmosphere:

$$L_{toa} = \frac{F}{W} \cdot \frac{A}{\pi} \cdot \frac{1}{100} \quad (7)$$

where  $L_{toa}$  is the radiance on top of the atmosphere ( $W m^{-2} \mu m^{-1} sr^{-1}$ ),  $F$  the integrated solar spectral irradiance weighted by the relative spectral response function of the sensor wavelength band  $W m^{-2}$ ,  $W$  the equivalent band width of the spectral response function of the sensor wavelength band [ $\mu m$ ], and  $A$  the Albedo [%].

After the calculation of the radiances for the VIS and NIR channels, they are corrected for atmospheric path radiance.

### Atmospheric Correction

Atmospheric effects can be corrected by a dark-target subtraction method if information on the state of the atmosphere is lacking (Richards, 1986; Kaufman and Sendra, 1988). Over a dark surface, path radiance constitutes the atmospheric effect. Path radiances for the red and near-infrared bands can be extracted from NOAA imagery by constructing radiance histograms for both channels and for the area of interest. Hence dark pixels were selected based on the radiometric properties of the surface of interest. The distance between the origin of the radiance histograms for the VIS and NIR channels, and the first 0.01% of nonzero radiance values were taken for the calculation of path radiances for both bands. By this procedure, densely forested surfaces are retained for the VIS channel and sea surface for the NIR channel. As an example, Figure 2 shows that for three of the seasons in 1990, dark pixels for the VIS channel, have a quite fixed geographical location and are associated with dense vegetation (e.g., forests). In order to visualize the dark pixels shown in this example, the first 1% of nonzero radiance values obtained from the radiance histogram were selected. The pattern of path radiance variation for both VIS and NIR is illustrated in Figure 3. Raw NDVI values, radiometrically calibrated values, and atmospherically corrected values are shown in Figure 4 for deciduous forest. An increase

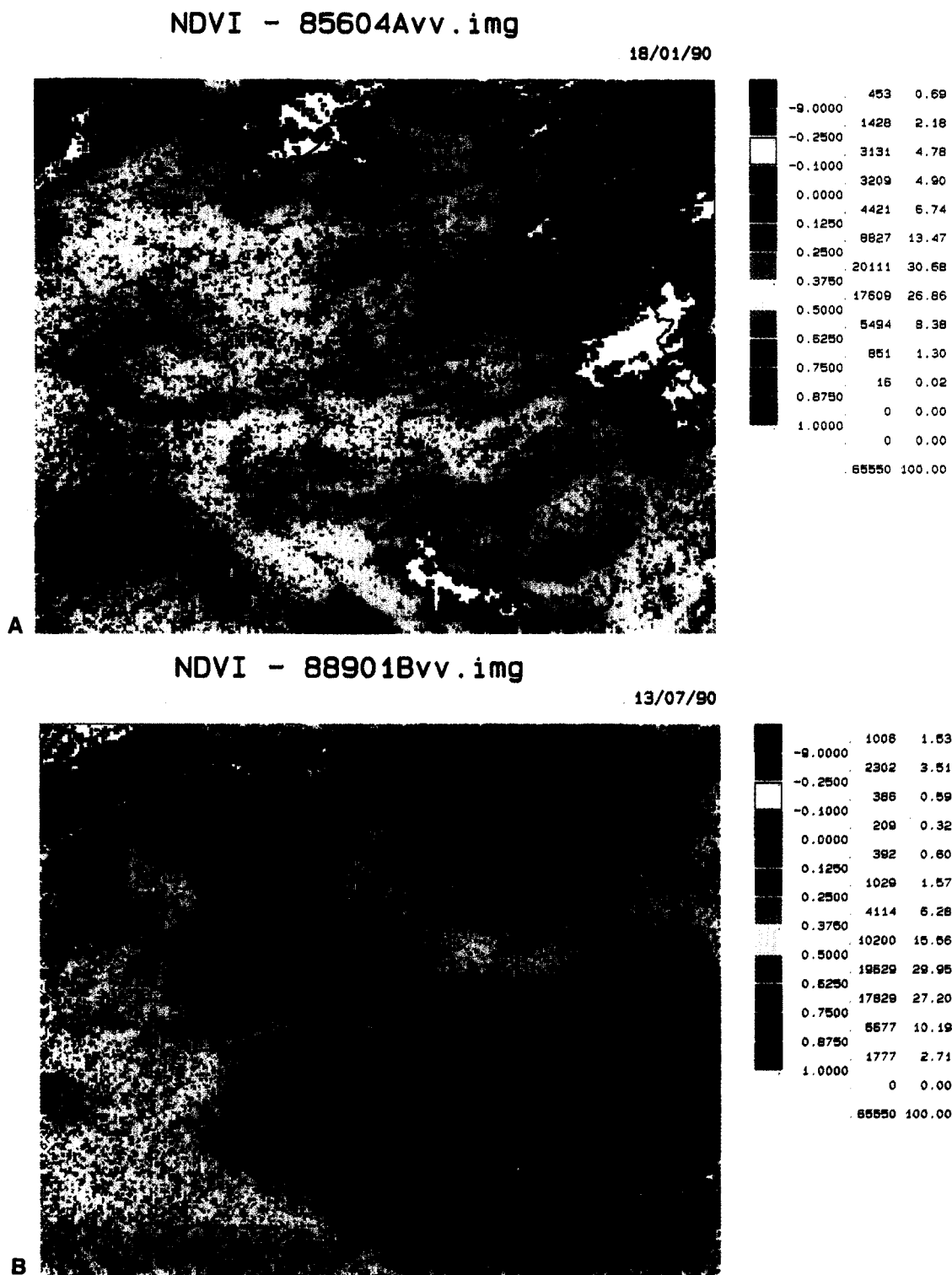


Figure 2. Top of atmosphere NDVI images for Belgium, obtained with the NOAA11-AVHRR / 2 for January (a), July (b), and October (c) 1990, show that the location of dark pixels (black dots) for different seasons coincides with dense vegetation (forest). They, moreover, are associated consistently with dense vegetation (forested areas), independent from the time of the year. The highest abundance during summer of dark pixels is an expected result.

NDVI - 90601Bvv.img

21/10/90

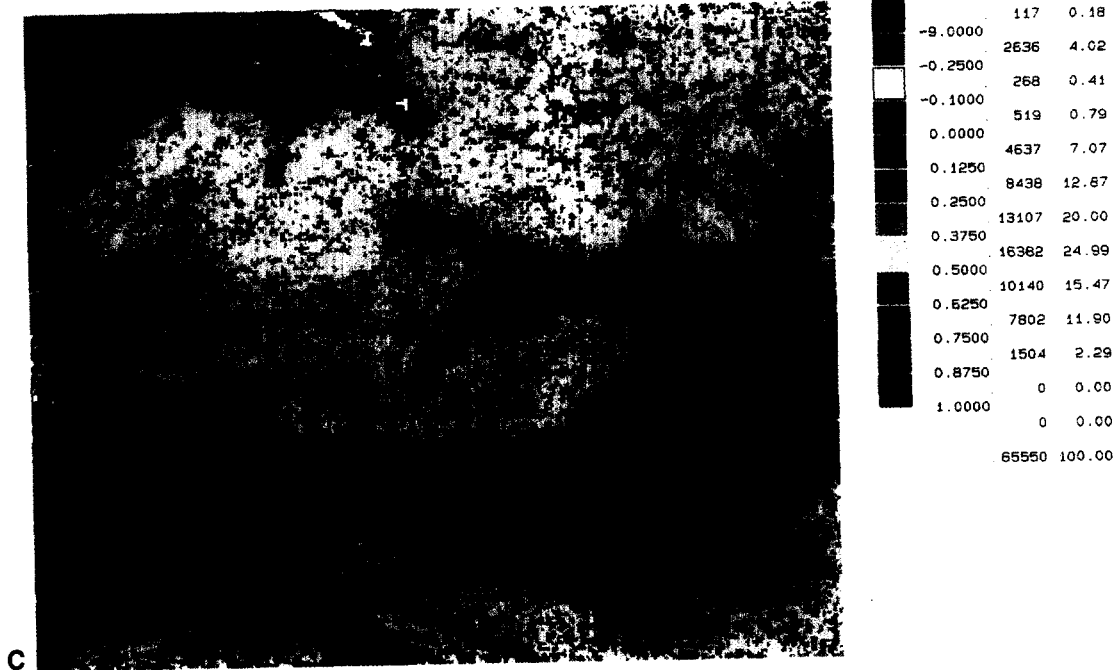


Figure 2. (continued)

in the dynamical range of the NDVI after atmospheric correction can be observed.

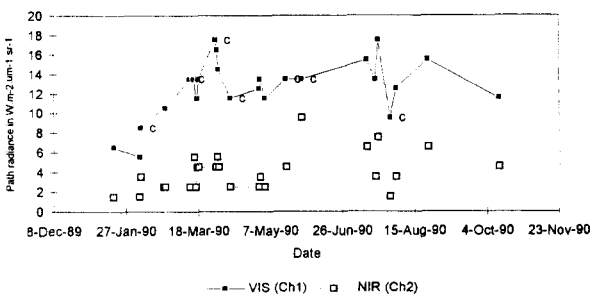
**THE RELATIONSHIP BETWEEN fPAR AND NDVI**

There is substantial empirical, and in some cases theoretical, evidence that vegetation indices are related to several vegetation parameters such as ground cover, leaf area index, radiation absorption, canopy photosynthesis, canopy conductance, etc. (Hall et al., 1992). From theoretical analysis it can be shown that TOC NDVI is, within some bounds, responsive to the leaf area in a canopy. Similarly, the amount of photosynthetically active radiation absorbed by the photosynthesizing tissue

(fPAR) is related to the green leaf area of the canopy. Thus, we may expect a causal relationship between TOC NDVI and fPAR (Asrar et al., 1984). The relationship between fPAR and TOC NDVI was found to be independent of pixel heterogeneity, parameterized with ground cover, clump leaf area index, and variations in leaf orientation and optical properties. On the other hand, it was sensitive to background, atmospheric, and bidirectional effects (Myneni et al., 1992a). Atmospheric and bidirectional effects, at vegetation level (TOC) as opposed to top-of-atmosphere (TOA), may be ignored if the analysis is limited to near-nadir TOC NDVI. Further, if the soils are moderately reflective, background effects may also be ignored. A linear model fits the resulting relationship between fPAR and TOC NDVI (see Fig. 5) significantly ( $r^2 = 0.943$ ,  $N = 280$ ). The slope of the relationship is 0.8465 (dimensionless) with an intercept of  $-0.1083$  (dimensionless). Thus the linear model gives a bare soil NDVI of 0.1279 (when fPAR = 0). This linear model or algorithm for fPAR is valid for: a) solar zenith angles less than  $60^\circ$ ; b) view zenith angles about the nadir; c) soils or backgrounds of moderate brightness (TOC NDVI of about 0.12); d) atmospheric optical depths less than 0.65 at 550 nm.

As an example, Figure 6 shows a regional fPAR map of Belgium for the 13 July 1990. The urban areas of Brussels, Antwerp and Gent show fPAR values close to zero. The agricultural areas of wheat east of Brussels show low fPAR values due to harvest. The densely forested area of the Ardennes shows high fPAR values.

Figure 3. Path radiances derived from histogram analysis of the 26 scenes of Belgium listed in Table 1 for the VIS and NIR bands of the NOAA11-AVHRR/2. The symbol (c) signifies presence of cloudy pixels in an image.



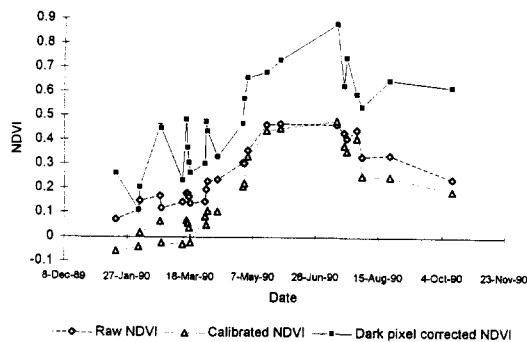


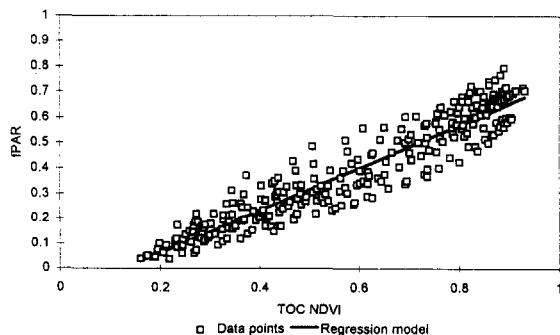
**Figure 4.** Comparison between raw, radiometrically calibrated and dark pixel corrected NDVIs, for a deciduous forest in Aulnoye, France. Dark pixel corrected NDVI profiles consistently show the highest levels and an enhanced dynamical range.

The Northern part of France shows low fPAR values due to wheat and other cereals that were harvested by this date. Typically pine forests in the Northern part of Belgium, with lower tree density due to regular thinning and cuttings, show lower fPAR values compared to the seminatural deciduous forests in the Ardennes.

#### FOURIER SERIES MODELING OF fPAR TEMPORAL PROFILES

To force ecosystem models with fPAR, temporal profiles of fPAR are derived from a discrete set of NOAA images. We used Fourier series to model the discrete temporal set of fPAR data, and secondly used the model to

**Figure 5.** The relationship between fPAR and the TOC NDVI, results from bright (sand) and dark (peat) soil sensitivity cases not included in this plot. A linear model fits the data significantly ( $r^2 = 0.943$ ,  $N = 280$ ). The slope of the relationship is 0.8465 (dimensionless) with an intercept of  $-0.1083$  (dimensionless). Thus the linear model gives a bare soil NDVI of 0.1279 (when fPAR = 0). This linear model or algorithm for fPAR is valid for: a) solar zenith angle less than  $60^\circ$ ; b) view zenith angles about the nadir; c) soils or backgrounds of moderate brightness (NDVI of about 0.12); d) atmospheric optical depths less than 0.65 at 550 nm.



retrieve fPAR values for each day of the year. Why do we need fPAR values for each day of the year? The ecosystem model is forced with daily fPAR values and since we only dispose of 26 fPAR values (out of 85 scenes in total, of which the remaining 59 were not cloudless) for the year 1990, Fourier series modeling is a necessary step for fPAR forcing of the ecosystem model. The procedure goes as follows.

Let fPAR(t) be a bounded function of period 2L satisfying the Dirichlet conditions a) in any period fPAR(t) is continuous, except possibly for a finite number of step discontinuities and b) in any period fPAR(t) has only a finite number of maxima and minima. With these constraints, fPAR(t) can be represented by a Fourier series:

$$fPAR(t) = \frac{a_0}{2} + \sum_{n=1}^{\infty} \left( a_n \cos \frac{n\pi \cdot t}{L} + b_n \sin \frac{n\pi \cdot t}{L} \right). \quad (8)$$

The first derivative of fPAR(t) is expressed as follows:

$$\frac{dfPAR(t)}{dt} = \sum_{n=1}^{\infty} \frac{n\pi}{L} \left( b_n \cos \frac{n\pi \cdot t}{L} + a_n \sin \frac{n\pi \cdot t}{L} \right). \quad (9)$$

The parameter t represents time and L the time interval between subsequent fPAR values, whereas  $a_0$ ,  $a_n$ , and  $b_n$  represent Fourier series coefficients which depend on the type of fPAR profile. The parameter n represents the number of harmonics.

The resulting fPAR temporal profiles for an agricultural area in Haspengouw (Belgium) and a deciduous forest in Aulnoye (France) are shown in Figure 7. The results show that a Fourier series with  $n=5$  fits the time series adequately. The first derivative clearly demonstrates the seasonal dynamics of fPAR, which are different for the agricultural area (Haspengouw) compared to the deciduous forest (Aulnoye).

#### NET ECOSYSTEM EXCHANGE OF CARBON USING REMOTE SENSING DERIVED fPAR AND AN ECOSYSTEM MODEL FOR DECIDUOUS FOREST

##### Description of an Ecosystem Model for Deciduous Forests

Since our prime goal is the forcing of an ecosystem model with remotely sensed fPAR, a model of carbon dynamics in a deciduous forest is used. The model proposed here is developed based on the approach of Janecek et al. (1989).

Four compartments are considered in the model, between which all carbon fluxes are evaluated. They can be classified according to seasonal phytomass changes in green and nongreen phytomass compartments and a litter compartment. Table 4 summarizes the classification. The green compartment (G) is representative of organs with large mass fluctuations (photosynthetically

active organs; assimilate storage organs, feeder roots, and fruits). The nongreen compartment (R) is representative of relatively small mass fluctuations (stems, branches, woody roots). The litter compartment (L) and the atmosphere, the last one, are considered here as an infinite source and sink. The process scheme resulting from the definition of the compartments is illustrated in Figure 8. Only the differences and additions in modeling approach as compared with Janecek's model will be described.

The model was implemented in MS-FORTRAN source code, compiled on a PC-platform (Compaq 386 / 25e) under MS-DOS 5.0 and the graphical interface Windows 3.1. For long-term simulations, compilation and running was performed on a DEC alpha workstation with OSF and X-Windows as graphical interface. A documented source code of the model and its input climatological file can be obtained on request from the author. Model results and graphical illustrations were processed and generated with a spreadsheet at PC level.

Carbon fluxes are expressed in  $\text{kg C m}^{-2} \text{h}^{-1}$ ,  $\text{kg C m}^{-2} \text{d}^{-1}$ , or  $\text{kg C m}^{-2} \text{y}^{-1}$ ,  $\text{m}^{-2}$  repercuting to ground surface area. S is a switching function that allocates assimilates into the green or nongreen phytomass compartments according to the phenological phase of the forest. The photosynthetic, respiratory, and other carbon fluxes defined in the model are driven by photosyn-

thetically active radiation flux (PAR), atmospheric temperature, day length, carbon dioxide and oxygen mixing ratios. The carbon fluxes are calculated on an hourly basis. Changes in phytomass and NEE are evaluated by integration on a daily basis.

The dependence of photosynthetic assimilation on varying fPAR, temperature as well as  $\text{CO}_2$  and  $\text{O}_2$  mixing ratios is formalized according to a product definition (Richter, 1985).

An essential element in the modeling exercise is the  $\text{CO}_2$  and  $\text{O}_2$  dependency of photosynthesis and the formalization of the  $\text{CO}_2$  fertilization effect. This problem is approached by incorporating Rubisco (Ribulose-bis-phosphate-carboxylase-oxygenase) enzymatic properties into the submodel for photosynthesis, which is an extension of the model of Janecek et al. (1989). A further model extension is the formalization and evaluation of litter fluxes, as well from the green and nongreen compartments towards the litter compartment ( $F_{gl}$ ,  $F_{rl}$ ) as from the litter compartment towards the atmosphere ( $F_{la}$ ).

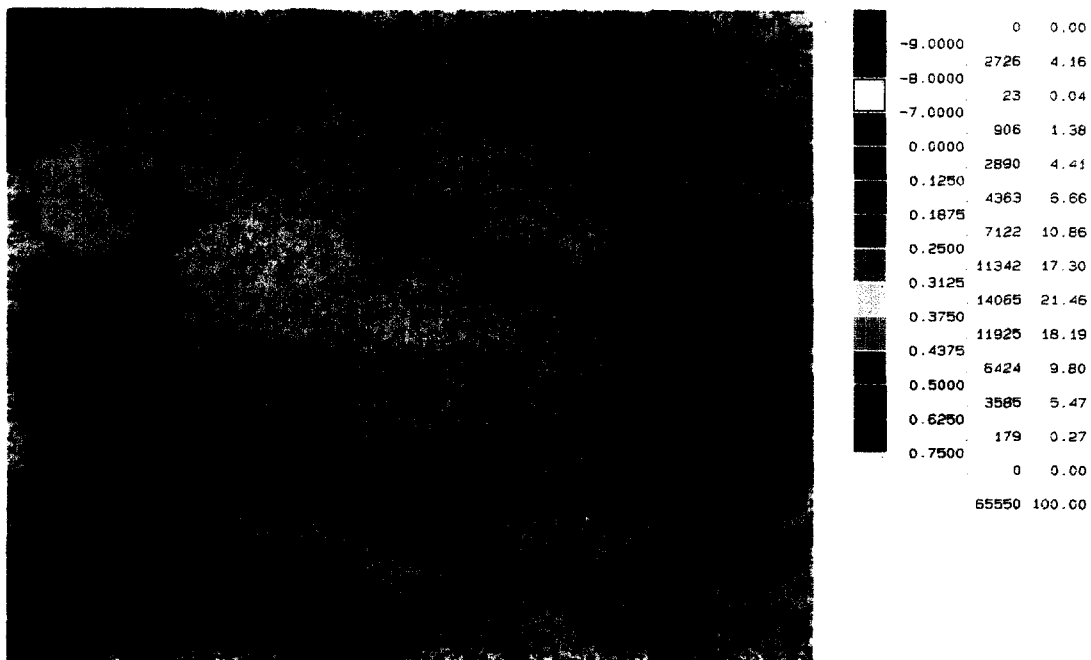
**Description of the Submodel for Photosynthetic Assimilation**

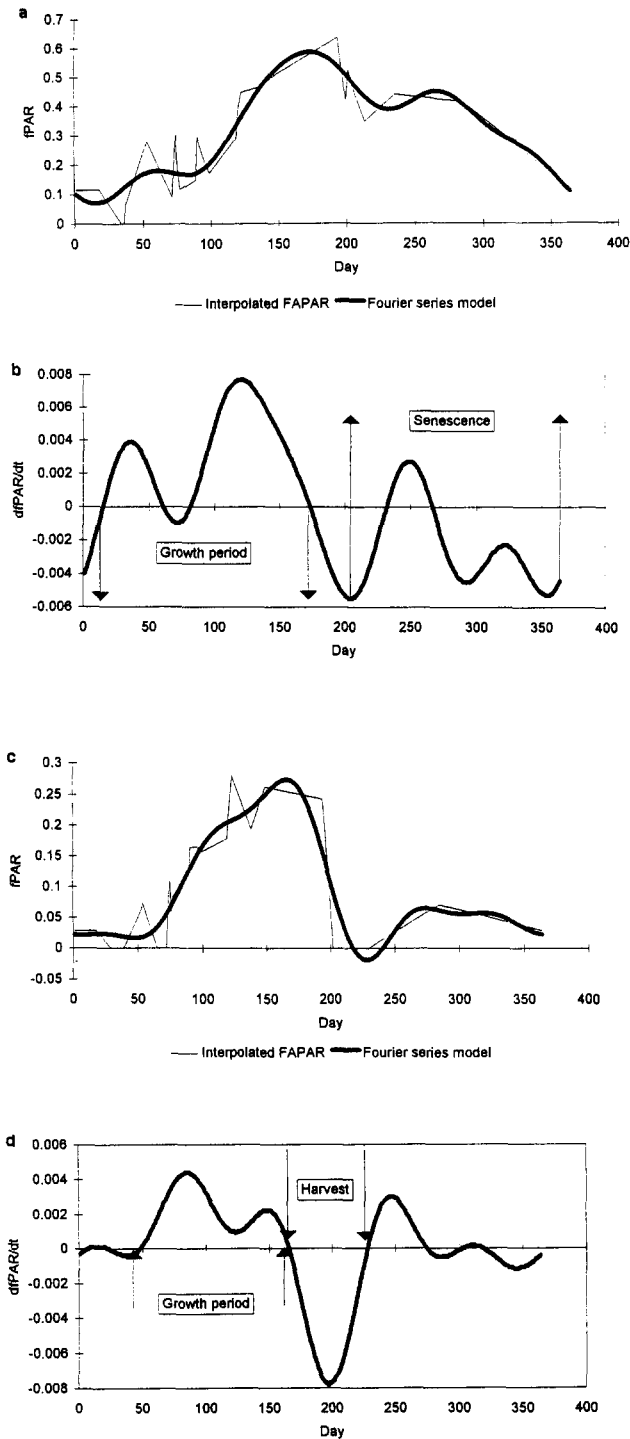
The critical forcing parameters for photosynthesis are PAR (photosynthetic active radiation), fPAR (the fraction of absorbed PAR), atmospheric temperature (T).

Figure 6. Regional fPAR map of Belgium during the summer period of 1990 (13 Th. of July) generated with NOAA11-AVHRR / 2 imagery from the VIS and NIR bands. fPAR values of 0.6–0.75 for seminatural forests in the Ardennes region, 0.0–0.1 for urban regions, and 0.4–0.5 for pine forests in the Northern part of Belgium are obtained based on the generalized fPAR–TOC NDVI relationship.

FAPAR - 88901Bfp.img

13/07/90





**Figure 7.** Fourier series model and temporal analysis of fPAR seasonal profiles of a deciduous forest (Aulnoye, France, a, b) and an agricultural area with mainly cereals in cultivation (Haspengouw, c, d). The residuals of measured and modeled fPAR values do not show a significant deviation from a Gaussian distribution (not shown).

the atmosphere  $\text{CO}_2$  and  $\text{O}_2$  mixing ratios, water and nutrient availability. The dependence of photosynthetic assimilation of fPAR, PAR, and temperature as well as  $\text{CO}_2$  and  $\text{O}_2$  dependence is formalized in a product

definition according to Richter (1985). To calculate photosynthetic assimilation, phytomass and NEE with fPAR profiles as RS-derived input parameter, the following relationship is applied:

$$p_1(\text{PAR}, \text{fPAR}) = C_u \times Q_{\text{eff}} \times \text{fPAR} \times \text{PAR}, \quad (10)$$

where  $C_u$  is the conversion factor for  $\text{mol CO}_2 \text{ m}^{-2} \text{ s}^{-1}$  to  $\text{kg C m}^{-2} \text{ h}^{-1}$  (with a value of 43.24),  $Q_{\text{eff}}$  the quantum efficiency ( $\text{mol CO}_2 \text{ E}^{-1}$ ) (with a value of 0.08 after Myneni et al. (1992b)), fPAR the fraction of absorbed PAR (dimensionless light absorption efficiency factor ranging from zero to 1), PAR photosynthetically active radiation ( $\text{E m}^{-2} \text{ s}^{-1}$ ,  $p_1$  temperature, and  $\text{CO}_2$  and  $\text{O}_2$  are independent gross photosynthetic assimilation,  $\text{kg C m}^{-2} \text{ h}^{-1}$ ). The application of Eq. (10) allows for the introduction of RS-derived fPAR into the ecosystem model.

### Dependence of Carbon Assimilation Rate on Temperature

A second product term  $p_2(T)$  is obtained by the application of a general model for the temperature dependency of complex plant physiological processes as formalized by Johnson et al. (1954). Lommen et al. (1974) used the model of Johnson et al. (1954) successfully in the evaluation of single leaf photosynthesis dependency on temperature. The formalization of Johnson et al. (1954) is a typical physiologically based approach with a generalization level allowing the most diverse applications in ecosystem modeling.

### Dependence of Carbon Assimilation Rate on $\text{CO}_2$ and $\text{O}_2$ Mixing Ratios

**Determination of the  $\text{CO}_2$  fertilization effect.** We can define the  $\text{CO}_2$  fertilization effect as the increase in carbon assimilation due to  $\text{CO}_2$  mixing ratios above the preindustrial background mixing ratio (reference level). The  $\text{CO}_2$  fertilization effect can be expressed on a relative basis to correct assimilation rates in comparison with the reference level.

The regression equation derived from data of Houghton and Woodwell (1989) to determine the  $\text{CO}_2$  mixing ratio for 1990, and used in the ecosystem model is:

$$[\text{CO}_2] = 1.175 \cdot \text{Year} - 1988 \quad (11)$$

valid for the period 1960–1990.

The  $R^2$  is 0.99. This equation obtained as a best fit for the data set referred to is applied here only to evaluate the  $\text{CO}_2$  mixing ratio for the year 1990, the year for which remote sensing data were processed. A mixing ratio of 350.2 ppmv is obtained and used in the calculation of the  $\text{CO}_2$  fertilization effect. The year 1990 falls within time period for which the equation is valid.

If  $[\text{CO}_2]^{\text{ref}} = 281 \text{ ppm}$ , the  $\text{CO}_2$  mixing ratio for the reference year 1833, we can formally express the effect of  $\text{CO}_2$  fertilization by:

Table 4. Classification of Functional Ecosystem Elements According to Their Seasonal Phytomass Changes

Large Mass Fluctuations, Green (G) Compartment	Relatively Small Mass Fluctuations	
	Nongreen (R) Compartment	Litter (L) Compartment
Photosynthetically active organs	Stems	Organic detritus from leaves, branches, stems and roots
Assimilate storage organs	Branches	
Feeder roots	Woody roots	
Flowers and fruits		

$$CO_2\text{effect} = \frac{F_{CO_2}}{F_{CO_2}^{ref}} \quad (12)$$

Evaluation of the temperature dependency of the CO<sub>2</sub> affinity coefficient  $K_m^{CO_2}$  according to Badger and Collatz (1976). The affinity coefficient  $K_m^{CO_2}$  shows a temperature dependence according to an Arrhenius relationship:

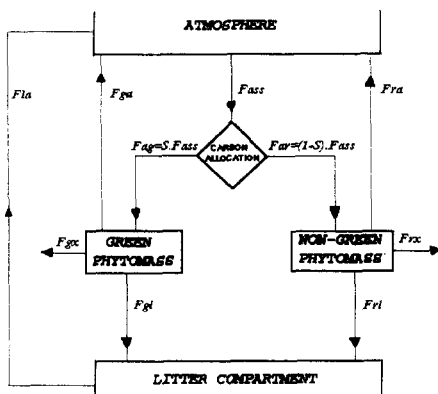
$$K_m^{CO_2} = Ae^{-E_a/R_{gas}T} \quad (13)$$

The Arrhenius plot is illustrated in Figure 9. For the calculation of coefficient A the following relationship is used:

$$\ln(A) = \ln(K_m^{CO_2}) + \frac{E_a}{R_{gas}} \cdot \frac{1}{T} \quad \text{for } T = 273.13 \text{ K.} \quad (14)$$

Since the temperature dependency shows two phases, originating from different conformational configurations for Rubisco in the chloroplast membrane, two sets of parameters are used in the model, depending on reigning temperature conditions. According to the two activation energies,  $E_{a1}$  and  $E_{a2}$ , for the two conformational phases the two constants  $A_1$  and  $A_2$  are determined by relation (14). The constants  $E_{a1}$ ,  $A_1$ ,  $E_{a2}$ , and  $A_2$  are applied to model the temperature dependence of  $K_m^{CO_2}$  according to Eq. (13).

Figure 8. Flow sheet illustrating the different compartments and carbon fluxes for a deciduous forest ecosystem model.



Final evaluation of the CO<sub>2</sub> fertilization effect. To finally evaluate the CO<sub>2</sub> fertilization effect, photorespiration is taken into account by assuming the following relationship for  $F_{CO_2}$  after Collatz et al. (1991).

$$F_{CO_2} = \frac{V_{max}([CO_2] - [O_2]/2\tau)}{K_m^{CO_2}(1 + [O_2]/2\tau) + [CO_2]} \quad (15)$$

where  $F_{CO_2}$  is the CO<sub>2</sub> assimilation rate,  $\tau$  the CO<sub>2</sub>/O<sub>2</sub> specificity ratio,  $K_m^{CO_2}$  the Rubisco affinity constant for CO<sub>2</sub>,  $K_0$  the inhibition constant for O<sub>2</sub>,  $V_{max}$  the maximal photosynthetic rate, and  $[CO_2]$  the CO<sub>2</sub> mixing ratio in the mesophyll tissue of leaves.

Substitution in relation (12) after elaboration gives

$$CO_2\text{effect} = p_3(CO_2, O_2) = \frac{[CO_2] - [O_2]/2\tau}{[CO_2]^{ref} - [O_2]/2\tau} \cdot \frac{K_m^{CO_2}(1 + [O_2]/K_0) + [CO_2]^{ref}}{K_m^{CO_2}(1 + [O_2]/K_0) + [CO_2]} \quad (16)$$

Table 5 summarizes the parameter values applied to model the CO<sub>2</sub> fertilization effect.

For  $K_m^{CO_2}$  the temperature dependency is applied as described earlier. For  $\tau$  and  $K_0$ ,  $Q_{10}$  values are converted to the Arrhenius constants  $E_a$  and  $A$ . We obtain for  $\tau$ :  $E_a = -42.8969$  (kJ mol<sup>-1</sup>) and  $A = 7.87 \cdot 10^{-5}$  [dimensionless]. For  $K_0$  we obtain:  $E_a = 13.9135$  (kJ mol<sup>-1</sup>) and  $A = 8.24 \cdot 10^3$  (% O<sub>2</sub>). These values are applied in the model to simulate the CO<sub>2</sub> and O<sub>2</sub> dependency of the carboxylation and oxygenation reactions of Rubisco.

Figure 9. Temperature dependence of  $K_m^{CO_2}$  according to Badger and Collatz (1976).  $E_{a1} = 59.4$  kJ mol<sup>-1</sup> for temperatures  $\geq 15^\circ\text{C}$  (288.13 K).  $E_{a2} = 109.6$  kJ mol<sup>-1</sup> for temperatures  $< 15^\circ\text{C}$  (288.13 K), where  $K_m^{CO_2} = 690$  ppmv (at 21.1°C or 294.23 K).

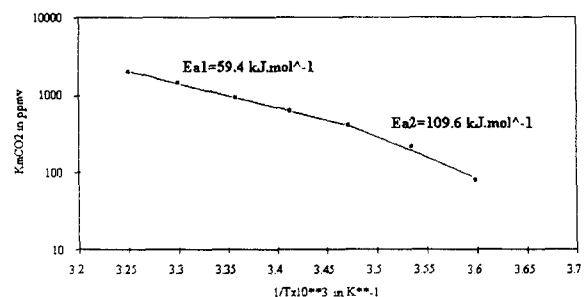


Table 5. Parameters Applied to Model the CO<sub>2</sub> Fertilization Effect

Parameter	Units	Value	Q <sub>10</sub>
$\tau$	Dimensionless	2600	0.57
K <sub>m</sub>	ppmv	690	2.1
K <sub>0</sub>	%	30	1.2
[O <sub>2</sub> ]	%	20.9	—
[CO <sub>2</sub> ] <sup>ref</sup>	ppmv	281	—

### Final Result for the Calculation of F<sub>ass</sub>, the Carbon Assimilation Rate

From the foregoing chapters we can combine the different expressions and dependencies of F<sub>ass</sub> on PAR, fPAR, T, CO<sub>2</sub>, and O<sub>2</sub> as follows:

$$F_{ass} = p_1(PAR, fPAR) \cdot p_2(T) \cdot p_3(CO_2, O_2). \quad (17)$$

Relationship (17) is applied for modeling photosynthetic assimilation rate as a function of PAR, fPAR, temperature, and CO<sub>2</sub> and O<sub>2</sub> mixing ratios. PAR as a function of global radiation is simulated with an astronomic model from Janecek et al. (1989). Temperature is taken from a historical record compiled by H. Poppe (in 1991).<sup>1</sup> CO<sub>2</sub> mixing ratios are taken from the Mauna Loa data set published by Houghton and Woodwell (1989). Daily fPAR values derived from Fourier series modeling are used to force the (deciduous forest) ecosystem model.

### Description of Submodels for Autotroph Respiration

Generally it is found that respiration is dependent on the mass of living tissues. Steady-state respiration is assumed proportional to tissue mass and is primarily dependent on temperature.

The modeling of autotroph respiration for the green phytomass compartment is straightforward knowing that there is no respiratory inactive phytomass fraction. For the nongreen compartment it is assumed that only part of the woody mass is respiring autotrophically. The ratio of living (respiring) wood to dead wood decreasing with increasing wood mass. For the description of the metabolizing wood fraction an empirical relationship was applied, based on typical values for actively respiring wood fractions from Strasburger (1985). The relationship obtained has the following form:

$$R_r(R) = (R + \Phi)^\gamma - \Psi. \quad (18)$$

R is a nongreen phytomass (kg C m<sup>-2</sup>) and R<sub>r</sub>(R) is the living part of nongreen phytomass [kg C m<sup>-2</sup>]. The parameters  $\Phi$ , (1.55 kg C m<sup>-2</sup>),  $\gamma$  (0.45, dimensionless), and  $\Psi$  (1.22 kg C m<sup>-2</sup>) are fitting constants.

Our previous considerations result in autotroph re-

Table 6. Parameter Values Applied for Modeling Respiratory Temperature Dependence [Function f(T)]<sup>a</sup>

Parameter	Units	Value
c	°K <sup>-1</sup>	0.59 × 10 <sup>6</sup>
ΔH*	J mol <sup>-1</sup>	4.985 × 10 <sup>4</sup>
ΔH <sub>1</sub>	J mol <sup>-1</sup>	1.8 × 10 <sup>5</sup>
ΔS	J °K <sup>-1</sup> mol <sup>-1</sup>	554.5
R <sub>gas</sub>	J °K <sup>-1</sup> mol <sup>-1</sup>	8.313

<sup>a</sup> Legend:

$$f(T) = \frac{cT \cdot e^{-\Delta H^*/R_{gas}T}}{1 + e^{-\Delta H_1/R_{gas}T} \cdot e^{\Delta S/R_{gas}}}$$

spiratory carbon fluxes F<sub>ga</sub> and F<sub>ra</sub>, respectively, from the green and nongreen compartments according to the following relationships:

$$F_{ga} = a_{GA} \cdot f(T) \cdot G, \quad (19)$$

$$F_{ra} = a_{RA} \cdot f(T) \cdot R_r(R), \quad (20)$$

with F<sub>ga</sub> and F<sub>ra</sub> in kg C m<sup>-2</sup> h<sup>-1</sup>, a<sub>GA</sub> (0.0045 h<sup>-1</sup>), a<sub>RA</sub> (0.0003 h<sup>-1</sup>), f(T) dimensionless temperature dependency factor according to Johnson et al.'s (1954) formulation (see Table 6), G (green phytomass), and R<sub>r</sub>(R) in kg C m<sup>-2</sup>.

Relationships (19) and (20) are applied to model autotroph respiration, a<sub>GA</sub> and a<sub>RA</sub> are rate constants relating carbon flux with phytomass (green and nongreen phytomass), and were determined from ecosystem analysis (Janecek et al., 1989). Green phytomass is obtained by ecosystem model forcing as described in a later subsection.

**Temperature dependency.** For both green and nongreen phytomass the relative temperature dependency factor f(T) for respiration is modeled, based on Johnson et al.'s (1954) model. The model, however, was fitted with data from Lommen et al. (1971) to obtain an autotroph respiration temperature dependency profile for temperate forests. In contrast to the modeling approach of Janecek et al. (1989) the model of Johnson et al. (1954) is used and fitted with data from Lommen et al. (1971). Table 6 summarizes the parameter values applied to model temperature dependency of respiration and includes the formal expression of Johnson's model.

### Litter Production and Carbon Losses to the Atmosphere

The fluxes of dead phytomass into the litter compartment are due to complex dependencies on physiological state, phenology, and climate. For deciduous forests, photoperiodic control of leaf initiation and abscission is taken into account. Different biotic and abiotic processes lead to other carbon losses from the green and nongreen compartments for example primary consumption by herbivores or forest fires. The assumption is made here that they occur at a constant rate, determining the fluxes F<sub>gx</sub> and F<sub>rx</sub>.

A submodel for litter decomposition was developed

<sup>1</sup> Klimatologische basiswaarden Vlaanderen, developed in collaboration with the Belgian Royal Meteorological Institute (KMI), public domain software package.

in as simple a way as possible, without omitting the prime determinants of the processes governing litter decomposition. The carbon flux from the litter compartment  $F_{la}$ , to the atmosphere is taken into account in this model. Baldocchi and Meyers (1991) determined the processes governing  $\text{CO}_2$  fluxes from deciduous forest floor soil in function of temperature and soil moisture content. They found that litter temperature accounts for 44% of the variance in  $\text{CO}_2$  efflux rates. So litter temperature is a fair indicator of  $\text{CO}_2$  efflux. Cool litter temperatures (below  $14^\circ\text{C}$ ) restrict efflux values below  $0.049 \cdot 10^{-3} \text{ kg C m}^{-2} \text{ h}^{-1}$ , whereas warmer temperatures yield a nonlinear increase in efflux rates, with maximum values approaching  $0.246 \cdot 10^{-3} \text{ kg C m}^{-2} \text{ h}^{-1}$ . These values according to the authors can be generalized for other deciduous forest types. The data of Baldocchi and Meyers (1991) were used to determine the rate constant of the litter carbon flux  $F_{la}$ . Temperature dependency of  $F_{la}$  was formalized with the model of Johnson et al. (1954) and fitted with data from Baldocchi and Meyers (1991).

#### Description of Carbon Allocation

A full description of the formalization of carbon allocation is given in Janacek et al. (1989).

#### Net Ecosystem Exchange of Carbon (NEE)

The net exchange of carbon between an ecosystem and the atmosphere, can formally be expressed by means of the fluxes defined in Figure 8. Atmospheric carbon fixation by the ecosystem is represented by the flux  $F_{ass}$ . After redistribution in the ecosystem through carbon allocation ( $F_{ag}$ ,  $F_{ar}$ ), autotrophic respiration generates two carbon fluxes back into the atmosphere originating from the green and nongreen compartments, for example,  $F_{ga}$  and  $F_{ra}$ .

An important flux determining NEE, originates from the decomposition of organic material in the litter compartment by bacterial and fungal heterotrophic respiration ( $F_{la}$ ). We developed a simple submodel for litter decomposition, taking into account the prime determinant of the processes governing decomposition to estimate NEE. The parameterization of the heterotrophic respiratory carbon flux is based on the temperature dependency of decomposition (Baldocchi and Meyers, 1991). Although it is recognized that soil moisture has a strong control over heterotrophic respiration rates, it was not taken into account in the deciduous forest model.

Our formalization, which is analogous to that of Bartlett et al. (1990), is based on the definition of the ecosystem compartments as defined earlier. It is expressed as

$$NEE = F_{ass} - \sum F_{ia}(i = g, r, l). \quad (21)$$

In expression (21), a subdivision is made between the

autotrophic and heterotrophic respiratory fluxes, respectively, from green, nongreen phytomass, and litter decomposition.

#### Ecosystem Model Forcing, Convergence Testing, and Model Output

The procedure outlined in this section enables the retrieval of phytomasses (for the different ecosystem compartments) and carbon fluxes when condition (22) is met. More explicitly this signifies that  $G_{max}$  and all daily mass and flux values correspond with the dynamics of the yearly fPAR profile.

The fPAR forcing procedure is performed by iterative runs of the deciduous forest ecosystem model with the boundary condition (22) for a given yearly fPAR profile:

$$\frac{dG_{max}}{di} = 0. \quad (22)$$

$G_{max}$  is the maximal green phytomass during one year cycle while  $i$  is the number of iterations. Explicitly condition (22) means that iterations for  $i = 1-n$  will proceed until the following condition is met:

$$|G_{max,i-1} - G_{max,i}| \leq \varepsilon \quad (\varepsilon = 0.001 \text{ kg C m}^{-2}). \quad (23)$$

$\varepsilon$  is a preset tolerance value on  $G_{max}$ .

This iterative procedure leads to a single solution for the state and rate parameters of the ecosystem model that are independent of the initial seed value for green phytomass ( $G_{in}$ ) and litter mass ( $L_{in}$ ). Figure 10 illustrates a convergence test for extreme  $G_{in}$  and  $L_{in}$  values, respectively. Final solutions for  $G$ ,  $R$ , and  $L$  are reached for  $G_{in}$  values of 0.001, 0.25, and 0.5  $\text{kg C m}^{-2}$ —the last value being a climax value—after 12, 5, and 17 iterations, respectively. The percentage standard deviation of the mean values for  $G$  ( $0.27 \text{ kg C m}^{-2}$ ) and for  $R$  ( $5.87 \text{ kg C m}^{-2}$ ), for the three  $G_{in}$  values are respectively 2.3% and 4.7%. The percentage standard deviation of the mean value for  $L$  ( $0.114 \text{ kg C m}^{-2}$ ), for the three  $G_{in}$  values is 10.5%. The final solutions for  $L$  for a  $G_{in}$  value of 0.25 and  $L_{in}$  values of 0.001, 0.012 and  $0.024 \text{ kg C m}^{-2}$  are also reached after five iterations. The percentage standard deviation on the mean value for  $L$  ( $0.110 \text{ kg C m}^{-2}$ ), for the three  $L_{in}$  values is 14.7%.

In the next figures (11 and 12) model outputs are shown for a forest in Aulnoye, France. The results are obtained by means of forcing with Fourier-modeled daily fPAR values and climatological data (hourly temperature). The input yearly fPAR profile (for 1990) is illustrated in Figure 7a). The input fPAR profile was derived from a dark pixel corrected daily NDVI profile (see Figure 4), according to the procedure as outlined in the previous section. Climatological data for 1990 are taken from a historical record compiled by Poppe

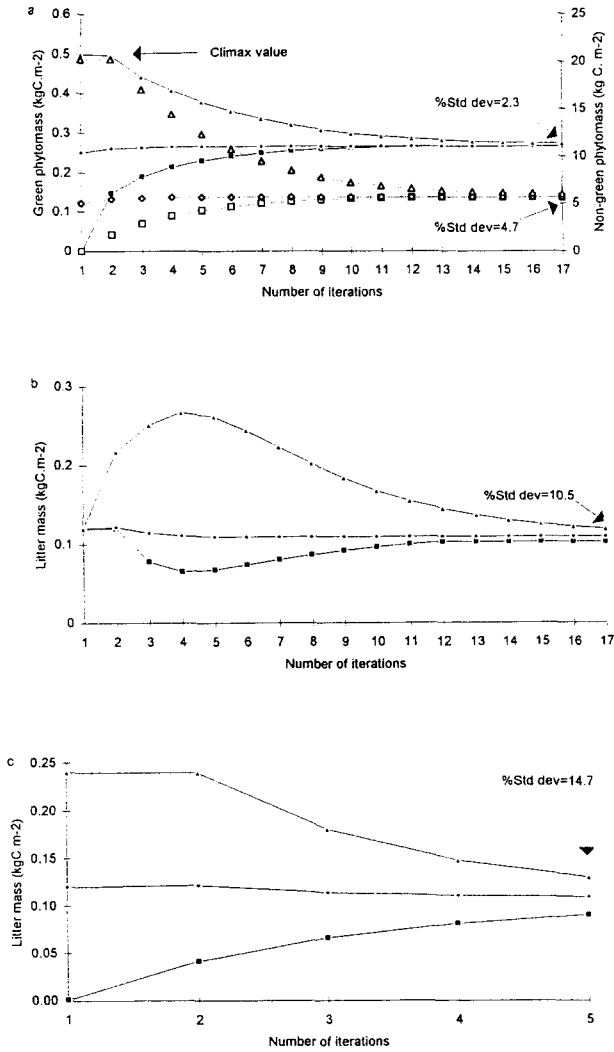


Figure 10. Convergence test for different seed  $G_{in}$  values, for green and nongreen phytomass (a), litter mass (b), and for different  $L_{in}$  values with a seed  $G_{in}$  value of 0.25 kg C m<sup>-2</sup> (c). a) Full line: green phytomass; dashed line: nongreen phytomass, rectangles  $G_{in} = 0.001$ , diamonds,  $G_{in} = 0.25$ , triangles  $G_{in} = 0.5$ . b) Rectangles  $G_{in} = 0.001$ , diamonds  $G_{in} = 0.25$ , triangles  $G_{in} = 0.5$ . c) Rectangles  $L_{in} = 0.001$ , diamonds  $L_{in} = 0.12$ , triangles  $L_{in} = 0.24$ .

1991.<sup>1</sup> CO<sub>2</sub> mixing ratios for 1990 were determined with the Mauna Loa data set published by Houghton and Woodwell (1989), and as explained in a previous subsection.

Figure 11 demonstrates phytomass and litter mass evolution as a function of time. Shooting and branching takes place from half February till April–May. Secondary growth proceeds till October, when foliage abscission starts. It can be concluded from these results that fPAR

<sup>1</sup> Klimatologische basiswaarden Vlaanderen, developed in collaboration with the Belgian Royal Meteorological Institute (KMI), public domain software package.

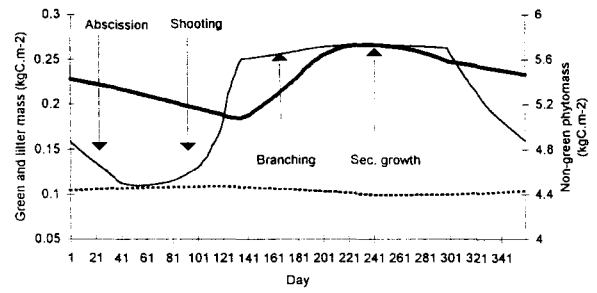


Figure 11. Green (G), nongreen (R), and litter (L) mass evolution for a deciduous forest (Aulnoye, France) after model forcing with a one pixel fPAR profile from the Aulnoye forest (fPAR profile shown in Fig. 7a).

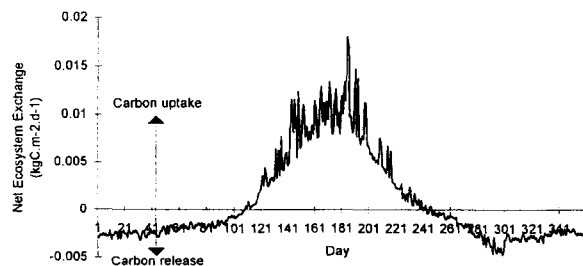
forcing of the model leads to a realistic sequence of the phenological phases for a deciduous forest.

During winter, early spring, and autumn, the respiratory fluxes from phytomass ( $F_{ga}$ ,  $F_{ra}$ ) and litter mass ( $F_{la}$ ) are responsible for a net release of carbon towards the atmosphere as illustrated in Figure 12, where NEE is negative during these periods. During summer a net uptake of carbon is apparent, due to photosynthetic activity exceeding the respiratory fluxes from the green, nongreen, and litter compartments.

Comparison of the NEE data from Figure 12 with those from Wofsy et al. (1993) for net exchange of CO<sub>2</sub> of a Mid-Latitude Forest in Petersham, Massachusetts, show good agreement with our results for the Aulnoye forest. During summer NEE for the Aulnoye and Petersham forests are respectively -0.009 and -0.0083 kg C m<sup>-2</sup> d<sup>-1</sup>. In wintertime values of respectively 0.0025 and 0.0015 kg C m<sup>-2</sup> d<sup>-1</sup> are obtained. This comparison indicates a reassuring concordance at flux level.

Young (1976) made a direct estimate of phytomass for a temperate deciduous forest located in Main (USA) at about 50° northern latitude, based on field measurements of 376 samples from the Elm Stream Township. Young (1976) obtained a total phytomass of 7.93 kg C m<sup>-2</sup>. Whittaker (1966; 1973) mentions a total phytomass range from 2.25 to 9 kg C m<sup>-2</sup> for young forests. For

Figure 12. Net ecosystem exchange (NEE) for a deciduous forest obtained after model forcing with a one pixel fPAR profile from the Aulnoye forest (fPAR profile shown in Fig. 7a).



many mature forests (climax state), the total phytomass ranges from 9 to 27 kg C m<sup>-2</sup>. Nabuurs and Mohren (1993) quantified stocks of carbon in Dutch forests based on inventory data and standing volume. A total phytomass in Dutch deciduous forest (more than 60 years old) of 6.27 kg C m<sup>-2</sup> was obtained. During the growing season, the maximal total phytomass was obtained with the fPAR forced model is 6.14 kg C m<sup>-2</sup>. Therefore our estimate is in good agreement with the results from Young (1976) and Nabuurs and Mohren (1993).

From the results of the latter it seems that litter mass on the forest floor (1.13 kg C m<sup>-2</sup>) is underestimated strongly by our procedure (we obtained a value of 0.114 kg C m<sup>-2</sup>). This may be due to an overestimate of the carbon flux towards the atmosphere from the litter compartment or by not taking into account the (mineralized) carbon in the soil compartment. A reevaluation of the rate constant for litter decomposition and incorporation of the carbon flux towards the unstable and stable carbon pools in the forest soil seems necessary for a good estimate of the heterotrophic respiration flux and hence NEE.

## CONCLUSIONS

A concept for coupling RS derived fPAR with a functional ecosystem model has been developed (the Belfix procedure). In the RS processing segment procedures have been developed for the geometric, radiometric and atmospheric correction of NOAA11/AVHRR2 data. A general relationship has been established between TOC NDVI and fPAR by means of 3D radiative transfer modeling at canopy level. Transportability of fPAR-TOC NDVI relationships was questioned by Bartlett et al. (1990), but theoretical work by Myneni et al. (1992a) demonstrates that this relationship is valid under a relatively wide spectrum of conditions. It is suggested that this relationship be applied to integrate fPAR in ecosystem models.

A Fourier series model has been developed to generate fPAR input datasets for ecosystem model forcing. In this publication the results obtained with fPAR forcing were presented. The modeling concept proved to be elaborate enough to generate phytomass, photosynthetic assimilation flux, autotrophic and heterotrophic respiratory fluxes, and NEE as outputs obtained with yearly fPAR profiles and climatological data. A good agreement between phytomass values, obtained with fPAR forcing of a deciduous forest model, and published phytomass values was obtained.

An interesting aspect of incorporating remote sensing derived fPAR in ecosystem models is that it has the potential for modeling actual as opposed to potential vegetation. The rationale for this is that we assume that fPAR is dependent on the longer term (weekly to

monthly) on the limiting factors of phytomass accumulation, as defined by Goudriaan (1994). We therefore suggest that remote sensing derived fPAR be incorporated in ecosystem models, because we assume that fPAR is a function of site-specific parameters, as for example nutritional status and water availability, which can be limiting for phytomass accumulation on the longer term. However, it has to be stated that the validity of the assumption that fPAR is a function of site-specific parameters is not demonstrated or tested in this publication. For example, we did not demonstrate that the modeling approach is valid in parts of Europe or the United States other than those mentioned in this publication. To test the validity of our assumptions, it is necessary to apply the modeling approach described in this publication for regions where soil fertility is low and where precipitation is limiting analogous to the work performed by Running and Nemani (1988) and Runyon et al. (1994).

---

*We are indebted to the valuable work and data processing efforts made by R. Smolders and E. Pastuer. This study is partly funded by the Belgian National Science Policy Office and carried out in the Global Change Impulse Programme, Contract GC/52/026. This support is gratefully acknowledged.*

## REFERENCES

- Asrar, G., Fuchs, M., Kanemasu, E. T., and Hatfield, J. H. (1984), Estimating absorbed photosynthetic radiation and leaf area index from spectral reflectance in wheat, *Agron. J.* 76:300-306.
- Badger, M. R., and Collatz, J. G. (1976), Studies on the kinetic mechanism of RudP-carboxylase and oxygenase, with particular reference to the effect of temperature on kinetic parameters, Carnegie Institution Annual Report, 1976-1977, Pittsburgh, PA.
- Baldocchi, D. D., and Meyers, T. P. (1991), Trace gas exchange above the floor of a deciduous forest, 1. Evaporation and CO<sub>2</sub> flux, *J. Geophys. Res.* 96(D4):7271-7285.
- Bartlett, S. B., Whiting, G. J., and Hartman, J. M. (1990), Use of vegetation indices to estimate intercepted solar radiation and net carbon dioxide exchange of a grass canopy, *Remote Sens. Environ.* 30:115-128.
- Cracknell, A. P., and Paithoonwattanakij, K. (1989), Pixel and subpixel accuracy in geometrical correction of AVHRR imagery, *Int. J. Remote Sens.* 10:661-667.
- Collatz, G. J., Ball, J. T., Grivet, C., and Berry, J. (1991), Physiological and environmental regulation of stomatal conductance, photosynthesis and transpiration: a model that includes a laminar boundary layer, *Agric. For. Meteorol.* 54:107-136.
- Goudriaan, J. (1994), Personal communication at the first GCTE Science Conference, Woods Hole, MA, May.
- Grime, J. P. (1979), *Plant Strategies and Vegetation Processes*, Wiley, Chichester.
- Hall, F. G., Huemmrich, K. F., Goetz, S. J., Sellers, P. J., and Nickeson, J. E. (1992), Satellite remote sensing of surface

- energy balance: Success, failures, and unresolved issues in FIFE, *J. Geophys. Res.* 97:19,061–19,089.
- Houghton, R. A., and Woodwell, G. M. (1989), Global climatic change, *Sci. Am.* 260:36–44.
- Janecek, O., Benderoth, A. G., Lüdeke, M. K. B., Kindermann, J., and Kohlmaier, G. (1989), Model of the seasonal and perennial carbon dynamics in deciduous type forests controlled by climatic variables, *Ecol. Model.* 49:101–124.
- Johnson, F. H., Eyring, H., and Polissary, M. J. (1954), *The Kinematic Basis of Molecular Biology*, Wiley, New York.
- Kaufman, Y. J., and Sendra, C. (1988), Algorithm for automatic corrections to visible and near-IR satellite imagery, *Int. J. Remote Sens.* 9:1357–1381.
- Lommen, P. W., Schwintzer, C. R., Yocum, C. S., and Gates, D. M. (1971), A model describing photosynthesis in terms of gas diffusion and enzyme kinetics, *Planta* 98:195–220.
- Myneni, R. B., Asrar, G., Tanré, D., and Choudhury, B. J. (1992a), Remote sensing of solar radiation absorbed and reflected by vegetated land surfaces, *IEEE Trans. Geosci. Remote Sens.* 30:302–314.
- Myneni, R. B., Ganapol, B. D., and Asrar, G. (1992b), Remote sensing of vegetation canopy photosynthetic and stomatal conductance efficiencies, *Remote Sens. Environ.* 42:217–238.
- Nabuurs, G. J., and Mohren, G. M. J. (1993), Carbon in Dutch forest ecosystems, *Neth. J. Agric. Res.* 41(4), forthcoming.
- Noble, I. R., and Slatyer, R. O. (1980), Use of vital attributes to predict successional changes in plant communities subject to recurrent disturbance, *Vegetation* 43:5–21.
- Prils, I. (1989), Geodetische Referentiesystemen, documents of the Belgian National Geographical Institute.
- Richards, J. A. (1986), *Remote Sensing Digital Image Analysis, An Introduction*, Springer-Verlag, Berlin, Heidelberg, pp. 40–41.
- Richter, O. (1985), *Simulation des Verhaltens Ökologischer Systeme—Mathematische Methode und Modelle*, VHC, Weinheim, 219 pp.
- Ruimy, A. (1995), Modélisation de la productivité primaire nette continentale, Ph.D. thesis, University of Paris-Sud, Centre D'Orsay.
- Running, S. W., and Nemani, R. B. (1988), Relating seasonal patterns of the AVHRR vegetation index to simulated photosynthesis and transpiration of forests in different climates, *Remote Sens. Environ.* 24:347–367.
- Runyon, J. (1994), Environmental limits on net primary production and light-use efficiency across the Oregon transect, *Ecol. Appl.* 4(2):226–237.
- Strasburger, E. (1985), *Lehrbuch der Botanik*, Fisher, Stuttgart, 1078 pp.
- Veroustraete, F. (1994a), Forcing of a simple ecosystem model with FAPAR and climatic data to estimate regional scale photosynthetic assimilation, in *Vegetation, Modelling and Climatic Change Effects* (F. Veroustraete et al., Eds.), SPB Academic, The Hague.
- Veroustraete, F. (1994b), On the use of simple deciduous forest model for the interpretation of climate change effects at the level of carbon dynamics, *Ecol. Model.* 75–76:221–237.
- Whittaker, R. H. (1966), Forest dimensions and production in the Great Smoky Mountains, *Ecology* 47:103–121.
- Whittaker, R. H., and Likens, G. E. (1973), in *Carbon in the Biota* (G. M. Woodwell and E. V. Pecan, Eds.), U.S.A.E.C., Washington, DC, pp. 281–302.
- Woodward, F. I. (1987), *Climate and Plant Distribution*, Cambridge University Press, Cambridge, 174 pp.
- Wofsy, S. C., Goulden, M. L., Munger, J. W., et al. (1993), Net exchange of CO<sub>2</sub> in a mid-latitude forest, *Science* 260:1314–1317.
- Young, H. E. (1976), Summary and analysis of weight table studies, in *Oslo Biomass Studies* (H. E. Young, Ed.), University of Maine, Orono.